When do tracer particles dominate the Lyapunov spectrum?

Pierre Gaspard
Center for Nonlinear Phenomena and Complex Systems, Université Libre de Bruxelles, Campus Plaine, Code Postal 231, 1050 Brussels, Belgium

Henk van Beijeren
Center for Nonlinear Phenomena and Complex Systems, Université Libre de Bruxelles, Campus Plaine, Code Postal 231, 1050 Brussels, Belgium
and
Institute for Theoretical Physics, Utrecht University, Leuvenlaan 4, 3584 CE Utrecht, The Netherlands
(February 8, 2008)

Dynamical instability is studied in a deterministic dynamical system of Hamiltonian type composed of a tracer particle in a fluid of many particles. The tracer and fluid particles are hard balls (disks, in two dimensions, or spheres, in three dimensions) undergoing elastic collisions. The dynamical instability is characterized by the spectrum of Lyapunov exponents. The tracer particle is shown to dominate the Lyapunov spectrum in the neighborhoods of two limiting cases: the Lorentz-gas limit in which the tracer particle is much lighter than the fluid particles and the Rayleigh-flight limit in which the fluid particles have a vanishing radius and form an ideal gas. In both limits, a gap appears in the Lyapunov spectrum between the few largest Lyapunov exponents associated with the tracer and the rest of the Lyapunov spectrum.

I. INTRODUCTION

During the last decade, dynamical instability and chaos in systems of interacting particles has become a problem of major preoccupation in statistical mechanics. Many systems have been shown to present sensitivity to initial conditions characterized by positive Lyapunov exponents [1,2]. Methods from kinetic theory have been developed for the maximal Lyapunov exponent and the Kolmogorov-Sinai entropy of dilute gases [3–8,**?**]. The relationships to transport properties have also been investigated [10–13].

In mixtures of a one-component fluid with a very low concentration of identical tracer particles the largest Lyapunov exponent may either be virtually identical to the largest Lyapunov exponent of the pure fluid (with just a slight perturbation caused by the tracer particles), or it may be larger, due to the dynamical properties of the tracer particles. In the latter case one may say that the largest Lyapunov exponent is *dominated by the tracer particles*.

The purpose of the present paper is to describe the regimes in which the tracer particles dominate the dynamical instability of the fluid system. If the mass of the tracer particle is not much larger than that of the fluid particles, and in addition the mean free path of both bath and tracer particles are at least comparable in length to their respective radii, the characteristic Lyapunov exponents for fluid and tracer dynamics respectively are roughly of the order of their respective collision frequencies. So in this case one may conclude that the tracer particle will dominate if its collision frequency is sufficiently larger than that of the fluid particles.

One obvious way to reach this goal is by making the mass ratio M/m of tracer mass over fluid particle mass very small. The limit where this ratio goes to zero corresponds to the Lorentz gas, for which the Lyapunov exponents of the tracer particle were derived several years ago [3,5,8].

Another common situation is where the radius of the tracer particles is much larger than that of the fluid particles, e.g., when one satisfies the conditions for Brownian motion, where also the mass of the tracer particle is much larger than that of the fluid particles. In this case the collision frequency of the tracer particles is much higher than that of

the fluid particles, but at the same time the velocity changes of the tracer particle in collisions with a bath particle are much smaller than those of the bath particles themselves. In addition the curvature of the Brownian particle, due to its large radius, is much smaller than that of a fluid particle and therefore the diverging effect (crucial for a positive Lyapunov exponent) of a Brownian-fluid collision is much smaller than that of a fluid-fluid collision. As a result of this the largest Lyapunov exponent usually is determined by the fluid particles, as noted both by Louis and Gaspard [14] and by Nasser and Dorfman [15]. However, there is one noteworthy exception to this, corresponding to the so-called Rayleigh-flight limit, where at fixed Brownian mass and radius the radius of the fluid particles is sent to zero. In the extreme limit of a Brownian gas surrounded by an ideal gas it is obvious that the Brownian particle has to dominate, as the Lyapunov exponents of the ideal gas are strictly zero. The goal of the present paper is thus to study these cases of dominance of the Lyapunov spectrum by the tracer particle.

The plan of the paper is the following. In Sec. II, the problem of dynamical instability in a system of hard balls of different masses and radii is posed. In Sec. III, we consider the Lorentz-gas limit. In Sec. IV, we consider the Rayleigh-flight limit. Conclusions are drawn in Sec. V.

II. THE DYNAMICAL SYSTEM AND ITS INSTABILITY

A. The dynamics

In this paper we will consider a system composed of many fluid particles and one tracer particle. From a general viewpoint, this system can be considered as a binary mixture of $N_{\rm f}$ fluid particles, which we take to be hard spheres of radius a and mass m, with $N_{\rm t}$ tracer particles, which will likewise be hard spheres, with radius A and mass M. All the $N = N_{\rm f} + N_{\rm t}$ hard balls move in a rectangular domain of finite extension Ω with periodic boundary conditions.

The motion of the hard balls is composed of free flights between binary collisions which are elastic and instantaneous. Energy and the total linear momenta are conserved.

For a system of hard balls of radii $\{a_i\}_{i=1}^N$ and of masses $\{m_i\}_{i=1}^N$, the equations of motion are given as follows in terms of the positions and velocities $\{\mathbf{r}_i^{(-)}(t_n), \mathbf{v}_i^{(-)}(t_n)\}_{i=1}^N$ and $\{\mathbf{r}_i^{(+)}(t_n), \mathbf{v}_i^{(+)}(t_n)\}_{i=1}^N$, respectively before and after the collision at time t_n:

1. Free flight between binary collisions:

$$t_{n-1} \to t_n : \quad \begin{cases} \mathbf{r}_i^{(-)}(t_n) \;=\; \mathbf{r}_i^{(+)}(t_{n-1}) \;+\; (t_n - t_{n-1})\; \mathbf{v}_i^{(+)}(t_{n-1}) \\ \mathbf{v}_i^{(-)}(t_n) \;=\; \mathbf{v}_i^{(+)}(t_{n-1}) \end{cases} \tag{1}$$

2. Binary collision:

$$t_n : \quad \mathbf{r}_i^{(+)} \;=\; \mathbf{r}_i^{(-)} \tag{2}$$

$$t_n : \quad \begin{cases} \mathbf{v}_i^{(+)} \;=\; \mathbf{v}_i^{(-)} \;-\; 2\, \frac{m_j}{m_i+m_j}\, (\boldsymbol{\epsilon}_{ij} \cdot \mathbf{v}_{ij}^{(-)})\, \boldsymbol{\epsilon}_{ij} \\ \mathbf{v}_j^{(+)} \;=\; \mathbf{v}_j^{(-)} \;+\; 2\, \frac{m_i}{m_i+m_j}\, (\boldsymbol{\epsilon}_{ij} \cdot \mathbf{v}_{ij}^{(-)})\, \boldsymbol{\epsilon}_{ij} \\ \mathbf{v}_k^{(+)} \;=\; \mathbf{v}_k^{(-)} \qquad\qquad \text{for} \quad k \neq i, j \end{cases} \tag{3}$$

with the unit vector joining the centers of the $i^{\rm th}$ and $j^{\rm th}$ balls at the collision given by

$$\boldsymbol{\epsilon}_{ij} \equiv \frac{\mathbf{r}_i^{(\pm)} - \mathbf{r}_j^{(\pm)}}{a_i + a_j} \tag{4}$$

and the relative velocity vector

$$\mathbf{v}_{ij}^{(-)} \equiv \mathbf{v}_i^{(-)} - \mathbf{v}_j^{(-)} \tag{5}$$

B. The linearized dynamics

The dynamical instability of this system is characterized by the rates of exponential growth of infinitesimal perturbations on the positions and velocities of the particles: $\delta\mathbf{X} = \{\delta\mathbf{r}_i, \delta\mathbf{v}_i\}_{i=1}^N$. The rates are called the Lyapunov exponents

$$\lambda = \lim_{t\to\infty} \frac{1}{t} \ln \frac{\|\delta\mathbf{X}(t)\|}{\|\delta\mathbf{X}(0)\|} \tag{6}$$

Depending on the initial perturbation $\delta\mathbf{X}(0)$ we may have as many different Lyapunov exponents as there are independent directions in phase space. Since the dynamics of the present hard-ball system is of Hamiltonian (symplectic) character the Lyapunov exponents obey a pairing rule: *If λ_i is a Lyapunov exponent, then $-\lambda_i$ is also a Lyapunov exponent.* The set of exponents form the so-called Lyapunov spectrum. The Lyapunov exponents associated with the directions perpendicular to the energy and momenta shells vanish. In the present system, which has no fixed points except at zero energy, this also holds for the pair mates associated with the directions of time and center-of-mass translation. Accordingly, $2 + 2d$ Lyapunov exponents vanish.

The problem of the dynamical instability of a hard-ball system was formulated in the seventies by Sinai [16] who was inspired by the pioneering work of Krylov in the forties [17]. Independently, Erpenbeck and Wood carried out numerical investigations, also in the seventies [18]. The systematic calculation of the Lyapunov spectrum in hard-ball systems has been developed in the nineties. Using the method of Gaspard and Dorfman [19] one can derive the following linearized equations in terms of the infinitesimal perturbations before and after each collision [14]:

1. Free flight between binary collisions:

$$t_{n-1} \to t_n : \quad \begin{cases} \delta\mathbf{r}_i^{(-)}(t_n) = \delta\mathbf{r}_i^{(+)}(t_{n-1}) + (t_n - t_{n-1})\, \delta\mathbf{v}_i^{(+)}(t_{n-1}) \\ \delta\mathbf{v}_i^{(-)}(t_n) = \delta\mathbf{v}_i^{(+)}(t_{n-1}) \end{cases} \tag{7}$$

2. Binary collision:

$$t_n : \quad \begin{cases} \delta\mathbf{r}_i^{(+)} = \delta\mathbf{r}_i^{(-)} - 2\, \frac{m_j}{m_i+m_j} (\boldsymbol{\epsilon}_{ij} \cdot \delta\mathbf{r}_{ij}^{(-)})\, \boldsymbol{\epsilon}_{ij} \\ \delta\mathbf{r}_j^{(+)} = \delta\mathbf{r}_j^{(-)} + 2\, \frac{m_i}{m_i+m_j} (\boldsymbol{\epsilon}_{ij} \cdot \delta\mathbf{r}_{ij}^{(-)})\, \boldsymbol{\epsilon}_{ij} \\ \delta\mathbf{r}_k^{(+)} = \delta\mathbf{r}_k^{(-)} \qquad \text{for} \quad k \neq i, j \end{cases} \tag{8}$$

$$t_n: \quad \begin{cases} \delta\mathbf{v}_i^{(+)} &= \delta\mathbf{v}_i^{(-)} - 2\,\frac{m_j}{m_i+m_j}\left[(\boldsymbol{\epsilon}_{ij}\cdot\delta\mathbf{v}_{ij}^{(-)})\,\boldsymbol{\epsilon}_{ij} + (\delta\boldsymbol{\epsilon}_{ij}\cdot\mathbf{v}_{ij}^{(-)})\,\boldsymbol{\epsilon}_{ij} + (\boldsymbol{\epsilon}_{ij}\cdot\mathbf{v}_{ij}^{(-)})\,\delta\boldsymbol{\epsilon}_{ij}\right] \\ \delta\mathbf{v}_j^{(+)} &= \delta\mathbf{v}_j^{(-)} + 2\,\frac{m_i}{m_i+m_j}\left[(\boldsymbol{\epsilon}_{ij}\cdot\delta\mathbf{v}_{ij}^{(-)})\,\boldsymbol{\epsilon}_{ij} + (\delta\boldsymbol{\epsilon}_{ij}\cdot\mathbf{v}_{ij}^{(-)})\,\boldsymbol{\epsilon}_{ij} + (\boldsymbol{\epsilon}_{ij}\cdot\mathbf{v}_{ij}^{(-)})\,\delta\boldsymbol{\epsilon}_{ij}\right] \\ \delta\mathbf{v}_k^{(+)} &= \delta\mathbf{v}_k^{(-)} \qquad \text{for} \quad k\neq i,j \end{cases} \tag{9}$$

with

$$\delta\boldsymbol{\epsilon}_{ij} = \frac{1}{a_i+a_j}\left(\delta\mathbf{r}_{ij}^{(-)} - \mathbf{v}_{ij}^{(-)}\,\frac{\boldsymbol{\epsilon}_{ij}\cdot\delta\mathbf{r}_{ij}^{(-)}}{\boldsymbol{\epsilon}_{ij}\cdot\mathbf{v}_{ij}^{(-)}}\right) \tag{10}$$

and

$$\delta\mathbf{r}_{ij}^{(-)} \equiv \delta\mathbf{r}_i^{(-)} - \delta\mathbf{r}_j^{(-)} \tag{11}$$

$$\delta\mathbf{v}_{ij}^{(-)} \equiv \delta\mathbf{v}_i^{(-)} - \delta\mathbf{v}_j^{(-)} \tag{12}$$

C. The kinetic properties of the thermodynamic equilibrium state

We require that the center of mass is at rest and we are interested in the properties of the equilibrium thermodynamic state at fixed temperature T. Accordingly, the total linear momenta vanish: $\mathbf{P}_{\rm tot} = \sum_{i=1}^N m_i\mathbf{v}_i = 0$, while the total energy is given by

$$E = \sum_{i=1}^N \frac{1}{2} m_i \mathbf{v}_i^2 = \frac{d}{2}(N-1)k_{\rm B}T \tag{13}$$

where $k_{\rm B}$ is Boltzmann's constant. For hard-ball systems, the motions at different temperatures are equivalent up to a rescaling of time. In the sequel, the temperature is thus fixed at the value $T = k_{\rm B}^{-1}$.

In the fluid phase at low enough density, the system is supposed to be ergodic on each energy-momenta shell, which defines the equilibrium states. The mean velocity[1] of each particle is defined as

$$v_i \equiv \langle \|\mathbf{v}_i\| \rangle \tag{14}$$

At equilibrium, the mean velocities are determined by the temperature and the mass of the particles. For large particle number, they are given, to leading order in $1/N$, by

$$d=2: \qquad v_i = \sqrt{\frac{\pi k_{\rm B}T}{2m_i}} \tag{15}$$

$$d=3: \qquad v_i = \sqrt{\frac{8k_{\rm B}T}{\pi m_i}} \tag{16}$$

where d is the space dimension.

---

[1] The mean velocity should be well distinguished from the root-mean-square velocity, defined as $\sqrt{\langle \mathbf{v}_i^2 \rangle}$.

The mean relative velocities between the particles entering a binary collision will also be of importance in the sequel. They are defined by

$$v_{ij} \equiv \langle \|\mathbf{v}_i - \mathbf{v}_j\| \rangle \tag{17}$$

and are given by Eqs. (15)-(16) with the mass replaced by the relative mass

$$\mu_{ij} \equiv \frac{m_i m_j}{m_i + m_j} \tag{18}$$

If the system is sufficiently dilute the collision frequencies of the fluid and tracer particles can be evaluated by supposing that each particle has a cross-section for collision with each one of the other types of particles:

$$d = 2: \qquad \sigma_{ij} = 2\,(a_i + a_j) \tag{19}$$

$$d = 3: \qquad \sigma_{ij} = \pi\,(a_i + a_j)^2 \tag{20}$$

If $\sigma_{\rm ff}$, $\sigma_{\rm ft} = \sigma_{\rm tf}$, and $\sigma_{\rm tt}$ denote the cross-sections for fluid-fluid, fluid-tracer, tracer-fluid, and tracer-tracer collisions, the collision frequencies of the tracer and fluid particles to leading order in the fluid density are given by

$$\nu_{\rm t} = \nu_{\rm tf} + \nu_{\rm tt} \simeq \frac{N_{\rm f}}{\Omega}\,\sigma_{\rm tf}\,v_{\rm tf} + \frac{N_{\rm t}-1}{\Omega}\,\sigma_{\rm tt}\,v_{\rm tt} \tag{21}$$

$$\nu_{\rm f} = \nu_{\rm ff} + \nu_{\rm ft} \simeq \frac{N_{\rm f}}{\Omega}\,\sigma_{\rm ff}\,v_{\rm ff} + \frac{N_{\rm t}}{\Omega}\,\sigma_{\rm ft}\,v_{\rm ft} \tag{22}$$

where $v_{\rm tf} = v_{\rm ft}$ and the extension parameter Ω is the area respectively the volume of the system:

$$d = 2: \qquad \Omega = L_x\,L_y \tag{23}$$

$$d = 3: \qquad \Omega = L_x\,L_y\,L_z \tag{24}$$

We notice that each tracer particle may collide on the $N_{\rm t} - 1$ other tracer particles, which explains the presence of -1 in the tracer-tracer collision frequency $\nu_{\rm tt}$. The term -1 is important in systems with a low number $N_{\rm t}$ of tracer particles. In contrast, it can be neglected if the number of particles is large as it is the case for the fluid particles.

D. Simulations and system preparation

In order to test our theoretical results we performed several MD simulations in which we computed the Lyapunov spectra of hard ball systems containing a tracer component. In all these simulations, we consider a fluid with a single tracer particle, so $N_{\rm t} = 1$.

To initialize a simulation we locate the fluid particles on the lattice points of a crystal lattice. In $d = 2$, the initial positions form a triangular lattice with $M_x M_y$ rectangular cells of two disks each. In $d = 3$, the initial positions form a face-centered cubic (FCC) lattice with $M_x M_y M_z$ cubic cells of four spheres each. The sizes of the cells are fixed in order for the fluid to have a fixed density n in absence of the tracer particle. In $d = 2$, the domain is rectangular of sizes

$$d = 2: \qquad L_x = M_x\,\left(\frac{2}{n\sqrt{3}}\right)^{\frac{1}{2}} \quad \text{and} \quad L_y = M_y\,\left(\frac{2\sqrt{3}}{n}\right)^{\frac{1}{2}} \tag{25}$$

so that its area is $\Omega = L_x L_y = 2M_x M_y/n$. In $d = 3$, the domain is also rectangular but of sizes

$$d = 3 : \qquad L_x = M_x \left(\frac{4}{n}\right)^{\frac{1}{3}} , \quad L_y = M_y \left(\frac{4}{n}\right)^{\frac{1}{3}} , \quad \text{and} \quad L_z = M_z \left(\frac{4}{n}\right)^{\frac{1}{3}} \tag{26}$$

so that its volume is $\Omega = L_x L_y L_z = 4M_x M_y M_z/n$.

Thereafter, the tracer particle is placed in the middle of the crystal configuration under removal of all the fluid particles that would overlap with the tracer particle. The number of fluid particles is thus given approximately by

$$N_{\rm f} \simeq n \, (\Omega - \Omega_{\rm t}) \tag{27}$$

where

$$d = 2 : \qquad \Omega_{\rm t} = \pi \, A^2 \tag{28}$$

$$d = 3 : \qquad \Omega_{\rm t} = \frac{4\pi}{3} \, A^3 \tag{29}$$

As a result of this procedure the density of the fluid particles in the *free volume* is still given to an excellent approximation by n, even if the tracer particle is so large that it occupies an appreciable fraction of the total volume Ω.

Accordingly, the collision frequency of the tracer particle is

$$\nu_{\rm t} = n \, \sigma_{\rm tf} \, v_{\rm tf} \tag{30}$$

and its mean free path is

$$\ell_{\rm t} = \frac{v_{\rm t}}{\nu_{\rm t}} \simeq \frac{v_{\rm t}}{n \, \sigma_{\rm tf} \, v_{\rm tf}} \tag{31}$$

Table I gives these quantities in $d = 2$ and $d = 3$.

Table I. Characteristic quantities for the motion of a tracer in a dilute fluid.

dimension	$d = 2$	$d = 3$
mean velocity	$v_{\rm t} = \sqrt{\frac{\pi k_{\rm B} T}{2M}}$	$v_{\rm t} = \sqrt{\frac{8 k_{\rm B} T}{\pi M}}$
collision frequency	$\nu_{\rm t} \simeq 2 \, (a + A) \, n \sqrt{\frac{\pi k_{\rm B} T (m+M)}{2mM}}$	$\nu_{\rm t} \simeq \pi \, (a + A)^2 \, n \sqrt{\frac{8 k_{\rm B} T (m+M)}{\pi mM}}$
mean free path	$\ell_{\rm t} = \frac{v_{\rm t}}{\nu_{\rm t}} \simeq \frac{1}{2 \, (a+A) \, n} \sqrt{\frac{m}{m+M}}$	$\ell_{\rm t} = \frac{v_{\rm t}}{\nu_{\rm t}} \simeq \frac{1}{\pi \, (a+A)^2 \, n} \sqrt{\frac{m}{m+M}}$

Finally, the initial velocities of the particles are drawn with a random number generator from a Maxwellian distribution with the appropriate mass. In practice we choose $k_B T = 1$ as well as $m = 1$.

E. Discussion of the dominance of the dynamical instability by the tracer

Since there is a single tracer particle it only collides with the fluid particles. However, each fluid particle may collide both with other fluid particles and with the tracer particle. Accordingly, there are two types of collisions: the fluid-fluid collisions and the tracer-fluid collisions.

Since both types of collisions happen between particles with convex surfaces, we expect that both of them will contribute to the dynamical instability. As discussed in the introduction, the strongest instability, characterized by the largest Lyapunov exponent, could be dominated either by the fluid-fluid collisions, or by the tracer-fluid collisions. To decide which of these possibilities is realized for a given choice of parameters we can proceed in the following way: We calculate both the fluid-fluid and the tracer-fluid maximal Lyapunov exponent *under the assumption that indeed fluid-fluid collisions repectively tracer-fluid collisions are dominant* and then compare the results. In the great majority of cases indeed the larger of the two calculated exponents gives an excellent approximation to the actual value of the maximal Lyapunov exponent.

The first calculation concerns the fluid-fluid collisions. In the absence of tracer, such collisions give the maximal Lyapunov exponent

$$\lambda_{\rm f} \simeq \omega(N_{\rm f})\ \nu_{\rm f}\ \ln\left[\frac{\alpha(N_{\rm f})}{4\,n\,a^d}\right] \qquad \text{with} \quad \nu_{\rm f} \simeq n\ \sigma_{\rm ff}\ v_{\rm ff} \tag{32}$$

where, for disks in $d = 2$, Van Zon *et al.* [6] have shown that the prefactor $\omega(N)$ is well fitted by the expression

$$\omega(N) \simeq 4.311 - \frac{3.466}{N^{0.277}}, \tag{33}$$

although the actual asymptotic behavior for large N is as $1/(\log N)^2$ [7]. Further, $\alpha(N_{\rm f})$ is of order unity, depends only weakly on $N_{\rm f}$ and approaches a constant for $N_{\rm f} \to \infty$.

On the other hand, we may consider the motion of the tracer particle undergoing kicks by independent fluid particles. The equations of motion are given by Eqs. (1)-(5) in which $\mathbf{r}_{i=1} = \mathbf{R}$, $\mathbf{v}_{i=1} = \mathbf{V}$. We denote by $(\mathbf{R}_n^{(-)}, \mathbf{V}_n^{(-)})$ and $(\mathbf{R}_n^{(+)}, \mathbf{V}_n^{(+)})$ the position and velocity of the tracer particle before repectively after the $n^{\rm th}$ collision, which occurs at the time t_n. Since the trajectory is continuous in position, $\mathbf{R}_n^{(+)} = \mathbf{R}_n^{(-)} \equiv \mathbf{R}_n$. On the other hand, $\mathbf{V}_n^{(+)} = \mathbf{V}_{n+1}^{(-)} \equiv \mathbf{V}_n$. We have the following iteration for the motion itself:

$$\mathbf{R}_n = \mathbf{R}_{n-1} + \tau_n\,\mathbf{V}_{n-1} \tag{34}$$

$$\mathbf{V}_n = \mathbf{V}_{n-1} - \frac{2\,m}{m+M}\,[\boldsymbol{\epsilon}_n \cdot (\mathbf{V}_{n-1} - \mathbf{v}_{n-1})]\,\boldsymbol{\epsilon}_n \tag{35}$$

$$t_n = t_{n-1} + \tau_n \tag{36}$$

where τ_n is the time interval between the $(n-1)^{\rm th}$ and the $n^{\rm th}$ collision, while

$$\boldsymbol{\epsilon}_n \equiv \frac{\mathbf{R}_n - \mathbf{r}_n}{A + a} \tag{37}$$

is the unit impact vector at the $n^{\rm th}$ collision.

An infinitesimal perturbation on the motion is ruled by Eqs. (7)-(12) in which $\delta\mathbf{r}_{i=1} = \delta\mathbf{R}$, $\delta\mathbf{v}_{i=1} = \delta\mathbf{V}$ and $\delta\mathbf{r}_j^{(\pm)} = \delta\mathbf{v}_j^{(\pm)} = 0$ for $j \neq 1$ because, if indeed the tracer particle dominates the maximal Lyapunov exponent, the perturbations of the fluid particle positions and velocities will be negligibly small compared to those of the tracer particle. For this argument to hold it is important that recollisions of a fluid particle with the tracer particle are either

rare, or, if they are not, are still dominated by the perturbations of the tracer particle. Especially when $M \gg m$ this is a subtle point, because, as can be seen from (7)-(12), the perturbations of a fluid particle right after a collision are comparable to those of the tracer particle. So if a recollision is not unlikely, it has to occur typically after a time that is long, compared to the Lyapunov time of the tracer particle. The iteration for an infinitesimal perturbation on the motion is then given by

$$\textit{free flight:} \qquad \delta\mathbf{R}_n^{(-)} = \delta\mathbf{R}_{n-1}^{(+)} + \tau_n\, \delta\mathbf{V}_{n-1} \tag{38}$$

$$\textit{binary collision:} \qquad \delta\mathbf{R}_n^{(+)} = \delta\mathbf{R}_n^{(-)} - \frac{2\,m}{m+M}\left(\boldsymbol{\epsilon}_n \cdot \delta\mathbf{R}_n^{(-)}\right)\, \boldsymbol{\epsilon}_n \tag{39}$$

$$\begin{aligned}\delta\mathbf{V}_n = \delta\mathbf{V}_{n-1} - \frac{2\,m}{m+M}\, \{&(\boldsymbol{\epsilon}_n \cdot \delta\mathbf{V}_{n-1})\, \boldsymbol{\epsilon}_n + [\delta\boldsymbol{\epsilon}_n \cdot (\mathbf{V}_{n-1} - \mathbf{v}_{n-1})]\, \boldsymbol{\epsilon}_n \\ &+ [\boldsymbol{\epsilon}_n \cdot (\mathbf{V}_{n-1} - \mathbf{v}_{n-1})]\, \delta\boldsymbol{\epsilon}_n\}\end{aligned} \tag{40}$$

with $\delta\mathbf{V}_n = \delta\mathbf{V}_n^{(+)} = \delta\mathbf{V}_{n+1}^{(-)}$ and

$$\delta\boldsymbol{\epsilon}_n = \frac{1}{A+a}\left[\delta\mathbf{R}_n^{(-)} - (\mathbf{V}_{n-1} - \mathbf{v}_{n-1})\, \frac{\boldsymbol{\epsilon}_n \cdot \delta\mathbf{R}_n^{(-)}}{\boldsymbol{\epsilon}_n \cdot (\mathbf{V}_{n-1} - \mathbf{v}_{n-1})}\right] \tag{41}$$

In the equations above, the perturbation $\delta\mathbf{R}_n^{(-)}$ corresponds to the first impact time of the two neighboring trajectories and the perturbation $\delta\mathbf{R}_n^{(+)}$ to the later impact time. They are related as

$$\delta\mathbf{R}_n^{(+)} = \delta\mathbf{R}_n^{(-)} + (\mathbf{V}_{n-1} - \mathbf{V}_n)\, \delta\tau_n\,; \tag{42}$$

with the time lag at collision

$$\delta\tau_n = -\frac{\boldsymbol{\epsilon}_n \cdot \delta\mathbf{R}_n^{(-)}}{\boldsymbol{\epsilon}_n \cdot (\mathbf{V}_{n-1} - \mathbf{v}_{n-1})} \tag{43}$$

These equations can be analyzed thanks to a few observations. First of all, the time τ_n between two successive collisions has an average value given as the inverse of the collision frequency of the tracer particle:

$$\langle \tau_n \rangle = \frac{1}{\nu_{\mathrm{t}}} \tag{44}$$

Furthermore, we find the mean relative velocity as

$$\langle \|\mathbf{V}_{n-1} - \mathbf{v}_{n-1}\| \rangle = v_{\mathrm{tf}} \tag{45}$$

We may expect a dominance of the resulting Lyapunov exponents for the tracer particle over those resulting from the fluid-fluid collisions in two cases to be discussed below: in the Lorentz-gas limit $M \to 0$ with $M \ll m$, and in the Rayleigh-flight limit $a \to 0$ with $a \ll A$ and $na^d \ll 1$. The calculation of these Lyapunov exponents will be the subject of the next two sections.

III. THE LORENTZ-GAS LIMIT

In the limit $M \to 0$, with $M \ll m$, the tracer particle is much faster than the fluid particles. Accordingly, the tracer moves through a fluid which is essentially at rest. This system is referred to as a Lorentz gas [20,21]. The collision

frequency of the tracer particle will thus be larger than the collision frequency of the fluid particles. Therefore, the perturbations on the coordinates of the tracer particle will grow faster than the perturbations on the fluid particles. Actually, the value of the maximal Lyapunov exponent of such a fluid can be predicted in this case thanks to the work by Van Beijeren, Dorfman, and Latz [3,5].

A. The two-dimensional case

In $d = 2$, the Lorentz gas has a single positive Lyapunov exponent as a consequence of chaos and energy conservation. Therefore, we expect that the maximal Lyapunov exponent is the positive Lyapunov exponent of the Lorentz gas when $M \ll m$, while the next Lyapunov exponents remain at the level of the fluid Lyapunov exponent (32). For a dilute system with $M \ll m$, the maximal Lyapunov exponent is therefore given by

$$d = 2 : \qquad \lambda_1 \simeq 2\,(a + A)\,n\,\sqrt{\frac{\pi k_{\mathrm{B}} T(m + M)}{2mM}}\;\ln\left[\frac{\mathrm{e}^{1-\mathcal{C}}}{2n(a + A)^2}\right] \tag{46}$$

with Euler's constant $\mathcal{C} = 0.5772156649...$ [3].

This behavior is well confirmed by numerical computation. Figure 1 compares Lyapunov spectra for $M \gg m$ and for $M \ll m$ at a fixed ratio of a and A. We observe that the maximal Lyapunov exponent is separated from the rest of the spectrum for $M \ll m$. This implies that with increasing m/M a gap opens up in the Lyapunov spectrum.

Figure 2 shows that in the limit $M \to 0$ the collision frequency of the tracer particle increases as predicted by Eq. (30) in the limit $M \to 0$.

Figure 3 depicts the five largest Lyapunov exponents as a function of the mass of the tracer particle showing that, indeed, the Lyapunov spectrum is dominated by the tracer particle as soon as $M \ll m$. The maximal Lyapunov exponent undergoes a cross-over from the fluid value (32) for $M \gtrsim m$ to the Lorentz-gas value (46) for $M \ll m$. In the regime $M \ll m$, the second Lyapunov exponent tends to slightly increase up to the fluid value (32) $\lambda_2 \simeq \lambda_{\mathrm{f}} < \lambda_1$. A similar behavior is seen for the next Lyapunov exponents.

Figure 4 shows the dependence of the spectrum on the radius A of the tracer particle. As the tracer becomes larger and larger in a fluid of fixed density, the room for its motion between the fluid particles becomes relatively smaller and smaller. A cage effect occurs for a large tracer as though the effective density of the Lorentz gas would increase (indeed the motion of a mobile particle of radius A among fixed point scatterers is completely equivalent to that of a mobile point particle among fixed scatterers of radius A that are allowed to overlap each other. In the literature this has been treated as the Lorentz gas with overlapping scatterers). In this case, the assumption $\ell_{\mathrm{t}}/A \gg 1$, on which the demonstration of (46) is based, breaks down, which explains the discrepancy observed in Fig. 4 for $A \gg a$ between the numerical results and the prediction of Eq. (46).

B. The three-dimensional case

In $d = 3$, the Lorentz gas has two positive Lyapunov exponents as a consequence of chaos and energy conservation. In this case, we thus expect that the two largest Lyapunov exponents are the positive Lyapunov exponents of the Lorentz gas when $M \ll m$, while the next Lyapunov exponents remain at the levels of the fluid Lyapunov exponents (32). For a dilute system with $M \ll m$, the two largest Lyapunov exponents are therefore given by [5]

$$d = 3 : \qquad \lambda_1 \simeq \pi\,(a + A)^2\,n\,\sqrt{\frac{8k_{\mathrm{B}} T(m + M)}{\pi mM}}\;\ln\left[\frac{4\,\mathrm{e}^{-\frac{1}{2}-\mathcal{C}}}{n\pi(a + A)^3}\right] \tag{47}$$

$$\lambda_2 \simeq \pi\,(a+A)^2\,n\,\sqrt{\frac{8k_{\rm B}T(m+M)}{\pi mM}}\;\ln\left[\frac{{\rm e}^{+\frac{1}{2}-\mathcal{C}}}{n\pi(a+A)^3}\right] \tag{48}$$

The next Lyapunov exponent should remain at the fluid value (32): $\lambda_3 \simeq \lambda_{\rm f} < \lambda_2 < \lambda_1$.

Here again, this behavior is well confirmed by numerical computation. Figure 5 depicts a Lyapunov spectrum for $M \ll m$ where we observe that, indeed, two Lyapunov exponents are separated from the rest of the spectrum, again with the formation of a gap as m/M increases. Figure 6 depicts the five largest Lyapunov exponents as a function of the mass of the tracer particle showing that the Lyapunov spectrum is dominated by the tracer particle as soon as $M \ll m$. The two largest Lyapunov exponents undergo a cross-over from the fluid values when $M \gg m$ to the Lorentz-gas values (47) and (48) for $M \ll m$. In the regime $M \ll m$, the third and next Lyapunov exponents tend to slightly increase up to the values of the first and next Lyapunov exponents of the previous regime $M \gg m$.

IV. THE RAYLEIGH-FLIGHT LIMIT

Another regime in which we may expect that the tracer particle dominates the Lyapunov spectrum is the one near the limit where the radius of the fluid particles vanishes: $a \to 0$. This regime can be characterized by the conditions $A \gg a$ and $na^d \ll 1$. In the limit, the fluid particles have no collisions between each other, but only with the tracer particle. This is referred to as the Rayleigh-flight limit and is known to present diffusive motion [22,23]. In the limit $a \to 0$ the fluid Lyapunov exponents (32) vanish. The tracer particle undergoes elastic, diverging collisions with the fluid. Since the tracer dynamics has d degrees of freedom, and the presence of the fluid particles precludes symmetry transformations of the tracer coordinates alone, we expect the existence of d positive Lyapunov exponents. In the Rayleigh-flight regime, we may thus expect that the dynamical instability of the fluid is dominated by the tracer particle, which is confirmed by the analysis given below. We want to remark here that the Rayleigh-flight limit provides an example of a system where the Lyapunov exponents remain well-defined in the infinite system limit. In fact taking this limit simplifies the analysis, because it largely limits the possibilities of recollisions.

A. Dynamical instability in the Rayleigh flight

Before considering the problem of the full fluid with $a \neq 0$, let us consider the dynamical instability of the tracer particle in an infinite domain filled with an ideal gas of fluid particles without mutual interaction. The fluid particles of mass m are coming from infinity with velocities distributed according to a Maxwell-Boltzmann distribution with temperature T and have a uniform spatial distribution with density n. In the limit $a \to 0$ the fluid particles have an infinite mean free path. The only possible collisions occur with the tracer particle. We notice that a fluid particle may collide more than once with the tracer particle. However, recollisions are rare if either of the conditions $M/m \gg 1$ or $l_{\rm t}/(A+a) \gg 1$ are satisfied. It will turn out that in order for the tracer particle to be dominant, at least one of these conditions has to hold and therefore we will neglect recollisions in the sequel.

At each collision, the velocity $\mathbf{v} = \mathbf{v}_{n-1}$ of the fluid particle is a random vector of Maxwell-Boltzmann distribution

$$P(\mathbf{v}) = \left(\frac{m}{2\pi k_{\rm B}T}\right)^{\frac{d}{2}}\;\exp\left(-\frac{m\mathbf{v}^2}{2k_{\rm B}T}\right) \tag{49}$$

Since the spatial distribution of the fluid particles is uniform the impact positions are distributed uniformly over the cross-section. If $\phi = \phi_n$ denotes the angle between the impact unit vector $\boldsymbol{\epsilon}_n$ with the relative velocity $\mathbf{v}_{n-1} - \mathbf{V}_{n-1}$

$$\cos\phi_n = -\frac{\boldsymbol{\epsilon}_n \cdot (\mathbf{V}_{n-1} - \mathbf{v}_{n-1})}{\|\mathbf{V}_{n-1} - \mathbf{v}_{n-1}\|}, \tag{50}$$

the uniform distribution of the impact positions implies that the collision angle is distributed according to

$$d = 2: \qquad P(\phi) = \cos\phi \tag{51}$$

$$d = 3: \qquad P(\phi) = \sin 2\phi \tag{52}$$

for $\phi \in \left[0, \frac{\pi}{2}\right]$. At low density and for $M \gg m$, the successive collisions undergone by the tracer particle occur at random time intervals $\tau = \tau_n$ which, for given speed $V = \|\mathbf{V}_{n-1}\|$ of the tracer particle are distributed according to an exponential probability distribution of mean intercollision time $\langle\tau(V)\rangle = 1/\nu_{\rm t}(V)$:

$$P(\tau) = \nu_{\rm t}(V)\ \exp\left[-\nu_{\rm t}(V)\tau\right] \tag{53}$$

In the limit $M/m \to \infty$ the velocity dependence of the collision frequency disappears.

If the recollisions are neglected, the parameters $(\mathbf{v}_{n-1}, \tau_n, \boldsymbol{\epsilon}_n)$ of the successive collisions are independent random variables, though for finite mass ratio their distribution does depend on the tracer speed V. Therefore, the tracer particle follows a random process which can be numerically simulated by a Monte-Carlo method. The growth factors of infinitesimal perturbations on the position and velocity of the tracer particle also follow a stationary random process.

Two regimes can be distinguished, depending on the value of the parameter

$$\gamma \equiv \frac{m}{M+m}\ \frac{1}{n(A+a)^d} \sim \sqrt{\frac{m}{M+m}}\ \frac{\ell_{\rm t}}{A+a} \tag{54}$$

This parameter is always smaller than the ratio of the mean free path $\ell_{\rm t}$ of the tracer particle to the collisional radius $A + a$ since $m/(m + M) \leq 1$.

For $\gamma \gg 1$ the dynamics in tangent space is very similar to that of a Lorentz gas. Typically the position perturbation of the tracer particle when entering a collision with a fluid particle, can be approximated by the product of its velocity perturbation and the free flight time since the previous collision. Since $\ell_{\rm t} \gg A + a$ in this case, the dynamical instability is essentially dominated by the large distance to the next collision that amplifies the perturbation on initial conditions by the ratio $\ell_{\rm t}/(A + a)$ (see Fig. 7a). Therefore, the maximal Lyapunov exponent can be calculated again by just considering the dynamics from one collision through the next one and averaging over the parameters of such an event. In fact, the Lorentz gas regime may be considered as a special subset of the class of all systems meeting the requirement $\gamma \gg 1$. This condition alone, together with the requirement that the resulting maximal tracer Lyapunov exponent exceeds the maximal fluid Lyapunov exponent, is sufficient to have dominance of the tracer particle.

For $\gamma \ll 1$ typically also the relative changes of the perturbations in a collision are much smaller than unity. A possible typical situation is illustrated in Fig. 7b in this case. Therefore, we may describe the dynamics in tangent space to a good approximation by a Fokker-Planck equation. Even though we have not found an analytical solution for this, we can infer several important properties from it, especially we can find out how the maximal Lyapunov exponent scales with the parameter γ.

(a) *The regime* $\gamma \gg 1$

In this regime, we can use Krylov's argument [17] to estimate the maximal positive Lyapunov exponent as follows. If $\gamma \gg 1$, Eq. (41) shows that a perturbation on the impact unit vector can be estimated as

$$\delta\boldsymbol{\epsilon}_n \sim \frac{\ell_{\rm t}}{A+a}\ \delta\theta_{n-1} \tag{55}$$

where $\delta\theta_{n-1}$ is a perturbation on the angle of the tracer velocity. If we substitute this estimation into Eq. (40) we can conclude that the perturbation on the tracer velocity angle should grow on average as

$$\delta\theta_n \sim \frac{m}{M+m}\,\frac{\ell_{\rm t}}{A+a}\,\frac{v_{\rm tf}}{v_{\rm t}}\,\delta\theta_{n-1} \sim \gamma\;\delta\theta_{n-1} \tag{56}$$

in a collision. Accordingly, the maximal Lyapunov exponent behaves as $\lambda_{\rm t} \sim \nu_{\rm t}\ln\gamma$.

The Monte-Carlo simulation confirms this expectation. Using the last expression of Table I in Eq. (56), we find that the numerical results for the maximal Lyapunov exponent of the tracer are well represented by

$$\gamma \gg 1: \qquad \lambda_{\rm t} \simeq \nu_{\rm t}\;\ln\left[\frac{m}{M+m}\;\frac{\alpha_{\rm t}}{n(A+a)^d}\right] \tag{57}$$

with the constant $\alpha_{\rm t} = \exp(1-\frac{3}{2}\mathcal{C})/(2\pi^{1/2}) = 0.322\ldots$, in the limit $M \gg m$ for $d = 2$. This agrees well with our simulation results, which give a fitting value for $\alpha_{\rm t}$ of 0.33 ± 0.05. In the Lorentz-gas limit $M \ll m$, the quantity $\alpha_{\rm t}$ also tends to a constant value, given by $\alpha_{\rm t} = {\rm e}^{1-\mathcal{C}}/2 = 0.763\ldots$ for $d = 2$, as may be seen from Eq. (46). The second positive Lyapunov exponent $\lambda'_{\rm t}$ turns out to have a different dependence on $A + a$ which we have not investigated theoretically yet.

(b) *The regime* $\gamma \ll 1$

In this regime, the dynamical instability is weaker. The perturbation on average only grows by a factor slightly larger than unity at each collision. From the Lyapunov instability, together with the relationship $\frac{d}{dt}\delta\mathbf{R} = \delta\mathbf{V}$, it is clear that, in the mean, the velocity and position perturbations of the Brownian particle are related through $\delta\mathbf{V} \sim \lambda_{\rm t}\delta\mathbf{R}$. Due to the Brownian fluctuations in the system, $\delta\mathbf{V}$ will in fact constantly fluctuate around the value $\lambda_{\rm t}\delta\mathbf{R}$, both in magnitude and in direction. To characterize these fluctuations we develop a continuous-time description of the dynamical instability similar to the one developed by Van Zon in another context [24]. We introduce the variables x and $\mathbf{y}$, defined through

$$x \equiv \frac{\delta\mathbf{R}\cdot\delta\mathbf{V}}{\delta\mathbf{R}^2} = \frac{\delta V_\parallel}{\|\delta\mathbf{R}\|} \tag{58}$$

$$\mathbf{y} \equiv \frac{\delta\mathbf{V} - x\,\delta\mathbf{R}}{\|\delta\mathbf{R}\|} = \frac{\delta\mathbf{V}_\perp}{\|\delta\mathbf{R}\|} \tag{59}$$

The variables x and $y \equiv \|\mathbf{y}\|$ describe the ratio's of velocity to position perturbations of the tracer particle, for the components parallel and perpendicular to $\delta\mathbf{R}$ respectively.

They allow us to obtain the maximal Lyapunov exponent as

$$\begin{aligned}\lambda_{\rm t} &= \lim_{T\to\infty}\frac{1}{T}\ln\frac{\|\delta\mathbf{R}(t)\|}{\|\delta\mathbf{R}(0)\|}\\ &= \lim_{T\to\infty}\frac{1}{T}\int_0^T dt\;\frac{d}{dt}\ln\|\delta\mathbf{R}(t)\|\\ &= \lim_{T\to\infty}\frac{1}{T}\int_0^T dt\;x(t)\end{aligned} \tag{60}$$

because

$$x = \frac{d}{dt} \ln \|\delta \mathbf{R}\| \tag{61}$$

and, again, $\frac{d}{dt}\delta\mathbf{R} = \delta\mathbf{V}$. Accordingly, the maximal Lyapunov exponent is given by the time average of the variable x. By ergodicity, this time average is equal to the statistical average over the stationary probability distribution of x:

$$\lambda_{\mathrm{t}} = \langle x \rangle \tag{62}$$

During each free flight between two collisions, the variables x and y have the form

$$x = \frac{a\tau + b}{a\tau^2 + 2b\tau + c} \tag{63}$$

$$y = \frac{\pm\sqrt{ac - b^2}}{a\tau^2 + 2b\tau + c} \tag{64}$$

with $\tau - t - t_{n-1}$ and

$$a = (\delta\mathbf{V}_{n-1})^2 \ , \qquad b = \delta\mathbf{R}_{n-1}^{(+)} \cdot \delta\mathbf{V}_{n-1} \ , \qquad \text{and} \quad c = (\delta\mathbf{R}_{n-1}^{(+)})^2 \tag{65}$$

The ratio x/y is a linear function of time so that

$$K \equiv \frac{d}{dt}\left(\frac{x}{y}\right) = \frac{x^2 + y^2}{y} \tag{66}$$

is a constant for the time evolution of x and y during the free flights. Without collisions, the variables x and y thus satisfy equations of motion

$$\begin{aligned} \dot{x}_{\mathrm{free}} &= -x^2 + y^2 = +y^2\,\partial_y K \\ \dot{y}_{\mathrm{free}} &= -2xy = -y^2\,\partial_x K \end{aligned} \tag{67}$$

However, the variables x and $\mathbf{y}$ undergo a jump at each collision of the tracer particle with the fluid particles. Accordingly, the time evolution of these quantities is ruled by the following coupled stochastic equations

$$\dot{x} = -x^2 + y^2 + \dot{x}_{\mathrm{coll}} \tag{68}$$

$$\dot{\mathbf{y}} = -2x\mathbf{y} + \dot{\mathbf{y}}_{\mathrm{coll}} \tag{69}$$

with

$$\dot{x}_{\mathrm{coll}} = \frac{\delta\mathbf{R} \cdot \delta\dot{\mathbf{V}}_{\mathrm{coll}}}{\delta\mathbf{R}^2} \tag{70}$$

$$\dot{\mathbf{y}}_{\mathrm{coll}} = \frac{\delta\dot{\mathbf{V}}_{\mathrm{coll}} - \boldsymbol{\rho}\,(\boldsymbol{\rho} \cdot \delta\dot{\mathbf{V}}_{\mathrm{coll}})}{\|\delta\mathbf{R}\|} \, , \tag{71}$$

where we introduced the unit vector

$$\boldsymbol{\rho} \equiv \frac{\delta\mathbf{R}}{\|\delta\mathbf{R}\|} \tag{72}$$

which is orthogonal to the unit vector $\boldsymbol{\sigma} \equiv \mathbf{y}/y$.

The jumps in the perturbation on the velocity are determined by Eq. (40) in the following form

$$\delta\dot{\mathbf{V}}_{\rm coll} = \sum_{n=-\infty}^{+\infty} (\delta\mathbf{V}_n - \delta\mathbf{V}_{n-1})\, \delta(t-t_n) \tag{73}$$

Accordingly, the collisional contributions (70)-(71) take the forms

$$\dot{x}_{\rm coll} = \sum_{n=-\infty}^{+\infty} \xi_n\, \delta(t-t_n) \tag{74}$$

$$\dot{\mathbf{y}}_{\rm coll} = \sum_{n=-\infty}^{+\infty} \boldsymbol{\eta}_n\, \delta(t-t_n) \tag{75}$$

To simplify our analysis we assume in the sequel that the mass ratio $m/(M+m)$ is very small.[2] As a result the relative velocity between tracer and fluid particles may be approximated by minus the velocity of the fluid particle, the collision frequency of the tracer particle becomes velocity independent and also the stationary distribution of the variables x and $\mathbf{y}$ becomes independent of the velocity of the tracer particle. The expressions for the jumps ξ_n and $\boldsymbol{\eta}_n$ simplify to leading order in $\frac{m}{M+m} \ll 1$. In particular, in Eq. (40) the terms proportional to $\delta\mathbf{V}$ may be neglected. In addition, in relative velocities the contributions of the tracer particle may be ignored. Using Eq. (40), we obtain, with these simplifications:

$$\xi_n \simeq \frac{2m}{(m+M)(a+A)}\, \|\mathbf{v}_{n-1}\|\, \left[\frac{(\boldsymbol{\epsilon}_n\cdot\boldsymbol{\rho}_n)^2}{\boldsymbol{\epsilon}_n\cdot\mathbf{u}_n} - \boldsymbol{\epsilon}_n\cdot\mathbf{u}_n\right] \tag{76}$$

$$\boldsymbol{\eta}_n \simeq \frac{2m}{(m+M)(a+A)}\, \|\mathbf{v}_{n-1}\|\, \left[\frac{(\boldsymbol{\epsilon}_n\cdot\boldsymbol{\rho}_n)^2}{\boldsymbol{\epsilon}_n\cdot\mathbf{u}_n}\,\boldsymbol{\rho}_n - \frac{\boldsymbol{\epsilon}_n\cdot\boldsymbol{\rho}_n}{\boldsymbol{\epsilon}_n\cdot\mathbf{u}_n}\,\boldsymbol{\epsilon}_n + (\boldsymbol{\rho}_n\cdot\mathbf{u}_n)\,\boldsymbol{\epsilon}_n - (\boldsymbol{\epsilon}_n\cdot\boldsymbol{\rho}_n)\,\mathbf{u}_n\right] \equiv \eta_n\,\boldsymbol{\tau}_n\,, \tag{77}$$

with the unit vector

$$\mathbf{u}_n \equiv -\frac{\mathbf{v}_{n-1}}{\|\mathbf{v}_{n-1}\|}, \tag{78}$$

and with $\boldsymbol{\tau}_n$ a unit vector orthogonal to $\boldsymbol{\rho}_n$. Since the successive jumps may be assumed to be statistically independent random variables, the time evolution in tangent space of an ensemble of tracer particles may be described by a *Boltzmann equation* for the distribution of x and $\mathbf{y}$, of the form

$$\partial_t f + \partial_x\left[(-x^2+y^2)f\right] + \partial_y\left[(-2xy)f\right] = \nu_{\rm t}\int_{-\infty}^{+\infty} d\xi \int_0^{\infty} d\eta \int' d\boldsymbol{\tau}\, \mathcal{P}(\xi,\eta,\boldsymbol{\tau})\, \left[f(x-\xi,\mathbf{y}-\eta\boldsymbol{\tau},t) - f(x,\mathbf{y},t)\right] \tag{79}$$

Here $\mathcal{P}(\xi,\eta,\boldsymbol{\tau})$ is the distribution function for jumps ξ and $\eta\boldsymbol{\tau}$ in x respectively $\mathbf{y}$ as result of a collision of the tracer particle with a fluid particle. The form of this distribution may be obtained from Eqs. (40)-(41), combined with the Maxwell distribution for the fluid particle velocity $\mathbf{v}_{n-1}$ and the distribution of the impact vector $\delta\boldsymbol{\epsilon}_n$ for given

[2]Even if this is not the case our main results, notably the way in which the maximal Lyapunov scales with γ, remain valid. But the specific analysis is more complicated, because the simplifications made at this point do not apply.

$\mathbf{V}_{n-1} - \mathbf{v}_{n-1}$. We used here that the terms in Eq. (40) proportional to $(\boldsymbol{\epsilon}_n \cdot \delta\mathbf{V}_{n-1})\ \boldsymbol{\epsilon}_n$ may be neglected, as result of which $\mathcal{P}(\xi, \eta, \boldsymbol{\tau})$ becomes independent of x and $\mathbf{y}$. This is justified because of our condition $\gamma \ll 1$, as can be seen on hindsight by comparing this term to the remaining terms in (40), approximating $\delta\mathbf{R}$ by $\delta\mathbf{V}/\lambda_{\rm t}$ in the latter [see Eqs. (76)-(77)]. The prime on the integral over $\boldsymbol{\tau}$ indicates an integration over the $d-1$-dimensional unit sphere orthogonal to $\boldsymbol{\rho}$. One readily sees that in fact $\mathcal{P}(\xi, \eta, \boldsymbol{\tau})$ as function of $\boldsymbol{\tau}$ is distributed uniformly over this unit sphere. Moreover, this distribution has long tails due to so-called *grazing collisions*, i.e., collisions with small scattering angles. As one sees from the second term in (41) these may give rise to arbitrarily large jumps in x and y of the order of

$$\xi_n\ ,\ \eta_n \sim \frac{\nu_{\rm t}\,\gamma}{\cos\phi_n} \tag{80}$$

As a consequence of the distribution (51), in $d = 2$, or (52), in $d = 3$ the tails of the probability density behave as

$$\mathcal{P}(\xi, \eta, \boldsymbol{\tau}) \sim \begin{cases} \frac{\nu_{\rm t}^2\,\gamma^2}{|\xi|^3} & \text{for } |\xi| \to \infty \\ \frac{\nu_{\rm t}^2\,\gamma^2}{|\eta|^3} & \text{for } |\eta| \to \infty \end{cases} \tag{81}$$

Therefore the first moments of this distribution exist. However, the slow decay of the distribution for large jumps leads to logarithmic divergences of the second moments of $\mathcal{P}$.

When the jumps in x and $\mathbf{y}$ at collisions are mostly small compared to the typical magnitudes of x and $\mathbf{y}$ themselves, it seems appropriate approximating the Boltzmann equation by a Fokker-Planck equation. For this to be the case we again need the condition $\gamma \ll 1$. But in addition, the approximation of the Boltzmann equation (79) by a Fokker-Planck equation requires the existence of the second moments of the distribution $\mathcal{P}(\xi, \eta, \boldsymbol{\tau})$. As we just noticed, these moments do not exist. But their divergence is only logarithmic and therefore the process, to leading order in γ, can still be described by a Fokker-Planck equation. The typical scale for the jumps in x and $\mathbf{y}$ is of order $\xi, \eta \sim \nu_{\rm t}\gamma$ with $\gamma \ll 1$. Consequently, if we introduce a cut-off in the calculation of the second moment at values of ξ and η satisfying

$$\xi_{\rm cut-off},\ \eta_{\rm cut-off}\ \sim\ \nu_{\rm t}\ \gamma^{1-\delta}, \tag{82}$$

with some $\delta > 0$, most of the distribution $\mathcal{P}$ falls within the cut-offs. We will justify this cut-off below by an argument of self-consistency, and at the same time determine the appropriate value of δ. Utilizing the cut-off, we obtain the following Fokker-Planck equation:

$$\partial_t f + \partial_x \left[(-x^2 + y^2 + \mu_\parallel) f\right] + \partial_y \left[(-2xy) f\right] = D_{\parallel\parallel}\ \partial_x^2 f + D_{\perp\perp}\ \partial_{\mathbf{y}}^2 f \tag{83}$$

where the drift in x is given by the first moment of the distribution $\mathcal{P}$ as

$$\mu_\parallel = \nu_{\rm t}\ \langle\xi\rangle \tag{84}$$

and the "diffusion coefficients" are defined as

$$D_{\parallel\parallel} = \frac{1}{2}\ \nu_{\rm t}\ \langle(\xi - \langle\xi\rangle)^2\rangle \tag{85}$$

$$D_{\perp\perp} = \frac{1}{2(d-1)}\ \nu_{\rm t}\ \langle\boldsymbol{\eta}^2\rangle \tag{86}$$

where d is the space dimension. There is no drift in $\mathbf{y}$ because $\langle\boldsymbol{\eta}\rangle = 0$ by symmetry. For the same reason, the coefficient of cross-diffusion in x and $\mathbf{y}$ vanishes.

Furthermore, in the limit $M/m \to \infty$ we are considering, one has $\langle\dot{\mathbf{V}}_{\rm coll}\rangle = 0$ by isotropy, irrespective of $\mathbf{V}$ and $\mathbf{R}$. Therefore also $\langle\delta\dot{\mathbf{V}}_{\rm coll}\rangle$ and, according to (70) and (74), $\langle\dot{x}_{\rm coll}\rangle$ and $\langle\xi\rangle$ vanish. A non-zero $\mu_\parallel$ may be obtained by

placing the Brownian particle in a harmonic well, a case we are investigating presently. ¿From the expressions (76) and (77) and the cut-offs (82) the diffusion coefficients may be estimated to behave as

$$D_{\|\|} = \frac{1}{2}\,\nu_{\rm t}\,\langle \xi^2\rangle \sim \nu_t^3\,\gamma^2\,\ln\frac{1}{\gamma}, \tag{87}$$

$$D_{\perp\perp} = \frac{1}{2(d-1)}\,\nu_{\rm t}\,\langle \boldsymbol{\eta}^2\rangle \sim \nu_t^3\,\gamma^2\,\ln\frac{1}{\gamma}, \tag{88}$$

Note that equation (83) has solutions that are independent of $\boldsymbol{\tau}$. It is precisely those solutions that we are interested in.

Continuing with hard spheres we note that, with vanishing first moments, the Fokker-Planck equation may be rescaled by applying the scalings $x \to x\,\kappa^{\frac{1}{3}}$, $\mathbf{y} \to \mathbf{y}\,\kappa^{\frac{1}{3}}$, and $t \to t\,\kappa^{-\frac{1}{3}}$. This allows us to extract the dependence of the variables on the expression $\kappa \equiv \nu_{\rm t}^3\gamma^2\ln(1/\gamma)$. The only remaining parameter that might change on varying the ratio's of masses and diameters is the ratio $D_{\perp\perp}/D_{\|\|}$. But even this will change just very slightly, and in fact only does so because the cut-offs on ξ and η in determining the second moments introduce a γ-dependence which works out somewhat differently for $D_{\|\|}$ and $D_{\perp\perp}$. In the limit $\kappa \to \infty$ this ratio has a well-defined limit.

From this scaling we may conclude immediately that $\langle x\rangle$, and hence the maximal Lyapunov exponent, scales as $\kappa^{1/3}$ and we finally obtain that

$$\lambda_{\rm t} = \langle x\rangle \sim \nu_{\rm t}\left(\gamma^2\,\ln\frac{1}{\gamma}\right)^{\frac{1}{3}} \tag{89}$$

with the parameter γ defined in (54).

A discussion is now in order to justify the introduction of the cut-off. As mentioned already, the second moments of the distribution $\mathcal{P}(\xi,\eta,\boldsymbol{\tau})$ diverge logarithmically. This implies that in principle we should stick with the Boltzmann equation (79). Still, the typical scale for the jumps in x and $\mathbf{y}$ is of order γ, whereas the typical scale for variations of x and $\mathbf{y}$ is expected to be at least approximately of order $\gamma^{2/3}$, so much larger. Therefore, the approximation of $f(x-\xi,\mathbf{y}-\eta\boldsymbol{\tau},t) - f(x,\mathbf{y},t)$ in (79) by a second order Taylor expansion should still be correct for values of $|\xi|$ and $|\eta|$ up to $c\gamma^{2/3}$, with c some small positive constant. In addition it can be estimated that the contributions to the Boltzmann equation from $|\xi|$- and $|\eta|$-values outside the cut-off are smaller by at least a factor of order $(\ln\frac{1}{\gamma})^{1/3}$ than the terms kept in the Fokker-Planck approximation. In this way, it is justified to introduce a cut-off of the form (82), with $\delta = \frac{1}{3}$, which establishes the self-consistency of the scheme.

The numerical computation shows that, indeed, the maximal Lyapunov exponent is of the form (89) for $\gamma \ll 1$, as seen in Fig. 8. The logarithmic correction turns out to be very small. We further observed that the second largest Lyapunov exponent also scales as (89).

Remark: The logarithmic divergences of the second moments of the distribution $\mathcal{P}$ are an anomaly of the hard-ball potential. For smooth potentials these moments are well-defined.

B. The full fluid dynamics

We now consider a fluid of small hard disks of radius $a = \frac{1}{2}$ and mass $m = 1$ with a tracer disk of radius A and mass M. The temperature is always $T = 1$. In order to find the conditions under which the tracer particle dominates the Lyapunov spectrum we proceed as follows.

We notice that the limit $a \to 0$ is equivalent to the conditions $A \gg a$ and $na^d \ll 1$. Therefore, we consider a sequence of systems of lower and lower density n. In the limit $n \to 0$, three types of tracer disks are considered:

$$(i)\ \ A=\frac{1}{2}\,,\qquad M=1, \tag{90}$$

$$(ii)\ \ A=5\,,\qquad M=100, \tag{91}$$

$$(iii)\ A=\frac{1}{2\sqrt{n}}\,,\ M=10. \tag{92}$$

The specific purpose of the last choice is to consider sequences of Brownian particles of increasing sizes, but all made of the same material, so the ratio of M to $nm(a+A)^2$ remains constant. In Fig. 9 the maximal Lyapunov exponent is plotted versus the density.

Case (i) is the reference situation in which all disks are identical and we recover the pure fluid behavior (32), as expected. Indeed, a best fit of the numerical data to a linear combination of $n\ln n$ and n yields

$$\lambda_{\rm f}=-10.9\ n\ \ln n-19.0\ n, \tag{93}$$

with the coefficient of the leading term in agreement with the value predicted by Eq. (32): $-2\sqrt{\pi}\,\omega(41)=-10.89$.

Both cases (ii) and (iii) are examples of Brownian motion, as both A/a and M/m are $\gg 1$. In case (ii) the parameter γ changes from $\gg 1$ for the larger of the density values considered to $\ll 1$ for the lowest densities. In case (iii) γ remains almost fixed at a value of $4/11$. The values of A/a and M/m chosen in case (ii) are such that the fluid always dominates the maximal Lyapunov exponent. This is clearly confirmed by the simulation results, which show that $\lambda_1\simeq\lambda_{\rm f}$.

In case (iii), in contrast, the tracer particle dominates the Lyapunov spectrum at low densities as observed in Fig. 9. Indeed, because $A=1/(2\sqrt{n})$, we infer from both Eq. (57) and (89) that

$$\lambda_{\rm t}\sim\nu_{\rm t}\sim\sqrt{n} \tag{94}$$

while the fluid Lyapunov exponent takes the values following from (93) so that $\lambda_{\rm f}\ll\lambda_{\rm t}$ for $n\to 0$. This explains the behavior observed in Fig. 9. We notice that case (iii) is intermediate between the two regimes, $\gamma\gg 1$ respectively $\gamma\ll 1$ studied in subsection IV A, because the mean free path of the tracer is only slightly smaller than the tracer radius. Indeed, in case (iii) we have $\ell_{\rm t}\simeq 0.3\,n^{-\frac{1}{2}}<A+a\simeq 0.5\,n^{-\frac{1}{2}}$. Therefore neither (57) nor (89) strictly applies, but the scaling of the maximal Lyapunov exponent as $\sqrt{n}$ remains valid.

However, with a system of one tracer disk among about 40 small disks, we are still in a situation very different from the Rayleigh flight because of the periodic boundary conditions and the boundedness of the domain. Even if the mean free path of the fluid particles among themselves is much larger than the size of the system $v_{\rm f}/\nu_{\rm ff}\gg L_x,L_y$ the fluid particles have recollisions on the tracer particle because of the periodic boundary conditions. When $(A/2a)^{d-1}\gg N_{\rm f}$ the dynamics of the fluid particles is dominated by recollisions with the tracer particle. We are then in a situation, similar to the Sinai billiard in which a point particle (such as a fluid particle) collides on a large disk (i.e., the tracer particle) in a system with periodic boundaries. This leads to two effects.

The first effect is that, in the limit where the tracer particle is very massive, the fluid particles become almost independent of each other. Therefore the Lyapunov spectrum becomes similar to $N_{\rm f}$ copies of the Lyapunov spectrum $(+\lambda_{\rm S},0,0,-\lambda_{\rm S})$ of the Sinai billiard. In the limit $M\to\infty$, we should thus expect a Lyapunov spectrum of the form $(\underbrace{+\lambda_{\rm S},...,+\lambda_{\rm S}}_{N_{\rm f}},\underbrace{0,...,0}_{2N_{\rm f}},\underbrace{-\lambda_{\rm S},...,-\lambda_{\rm S}}_{N_{\rm f}})$ in $d=2$. This tendency is indeed observed in Fig. 10 which compares two systems of different sizes with an identical tracer particle and at the same density. We observe in Fig. 10 that indeed the positive Lyapunov exponents roughly separate into two equally populated families. This tendency is stronger for the 40-particle system than for the 80-particle one, as was to be expected in view of the preceding arguments. In the limit $L_x,L_y\to\infty$, we notice that the Lyapunov exponent of the Sinai billiard vanishes as $\lambda_{\rm S}\sim(v_{\rm f}/L_{x,y})\ln(L_{x,y}/A)$ so that this effect tends to disappear.

The second effect due to the periodic boundary conditions is more important for our present considerations than the previous one. If the recollisions of a fluid particle with the tracer particle become more frequent than collisions with other fluid particles these may have an important, or even dominant effect on the growth of the perturbations on the tracer coordinates. As a consequence, the maximal Lyapunov exponent of the system may be different from the Rayleigh-flight value even though the tracer particle dominates and controls it. This effect may even remove the gap in the Lyapunov spectrum, as seen in Fig. 10. Notice that a small but finite density of large tracer particles will have exactly the same type of effects on the Lyapunov spectrum of a large or even infinite system as periodic boundary conditions in the case of a single tracer particle.

In the limit where the system becomes infinite, we expect that both effects disappear and that a gap does appear in the Lyapunov spectrum. This is indeed the case, as observed in Fig. 11 showing the five largest Lyapunov exponents for systems with the same density $n = 10^{-8}$ and temperature $T = 1$, the same tracer particle of radius $A = 5000$ and mass $M = 10$, but an increasing total size and so an increasing number $N_{\rm f}$ of fluid particles. Under these conditions, the limiting Rayleigh flight would have the following two positive Lyapunov exponents, obtained by Monte-Carlo simulation:

$$\begin{aligned} &d = 2\,,\ n = 10^{-8}\,,\ T = 1\,,\ A = 5000\,,\ M = 10\,: \\ &\lambda_{\rm t} = (3.3 \pm 0.1) \times 10^{-5}\,, \quad \lambda'_{\rm t} = (0.6 \pm 0.1) \times 10^{-5} \end{aligned} \tag{95}$$

For the full dynamics simulated by molecular dynamics, we observe in Fig. 11 that the maximal Lyapunov exponent decreases as $N_{\rm f} \to \infty$ to a value close to the maximal Lyapunov exponent $\lambda_{\rm t}$ of the Rayleigh flight. The next exponents decrease faster, creating a gap in the Lyapunov spectrum. We notice that, for the systems we studied, the second exponent has not yet converged to the Rayleigh-flight value $\lambda'_{\rm t}$ and is therefore not separated from the third and next exponents, but we expect this to occur for $N_{\rm f}$ large enough.

In the Rayleigh-flight limit, $a \to 0$, combined with the large system limit $N_{\rm f} \to \infty$, we therefore find a Lyapunov spectrum that is dominated by the dynamical instability of the tracer particle:

$$\lambda_1 \simeq \lambda_{\rm t} > \lambda_2 \simeq \lambda'_{\rm t} \gg \lambda_3 > \lambda_4 > ..., \tag{96}$$

with the formation of a gap, as in the case of the Lorentz-gas limit, but here because of a very different mechanism.

V. CONCLUSIONS

In this paper, we have studied a system of hard balls in elastic collisions (disks in $d = 2$ and spheres in $d = 3$) and we have shown that the tracer particle dominates the Lyapunov spectrum in the Lorentz-gas and in the Rayleigh-flight limit.

In the Lorentz-gas limit, the tracer particle is lighter and moves faster than the fluid particles. The tracer particle therefore has a higher collision frequency than the other particles. Since the maximal Lyapunov exponent is proportional to the collision frequency, a gap appears in the Lyapunov spectrum between the largest Lyapunov exponents, which are associated with the tracer particle, and the rest of the spectrum. In $d = 2$, there is one such positive Lyapunov exponent associated with the tracer and, in $d = 3$, there are two such exponents. These largest Lyapunov exponents take values very close to the Lorentz-gas values previously obtained by Van Beijeren, Dorfman, and Latz [3,5], as confirmed by direct numerical computation.

The other limit in which the tracer particle dominates the Lyapunov spectrum is the Rayleigh-flight limit. In this limit, the radius of the fluid particles tends to zero or, equivalently, the density of the fluid particles vanishes while the radius of the tracer is much larger than the radius of the fluid particles. In an infinite system, the only collisions would occur between the fluid particles and the lone tracer particle. We have shown the remarkable result that, even

in this limit where the fluid is ideal and composed of non-interacting particles, the tracer particle may have positive Lyapunov exponents. We obtained formulas for the dependence of the maximal Lyapunov exponent on the parameters of the system in two different regimes. In the first regime, where the mean free path of the tracer particle is so much larger than its radius that perturbations of its coordinates are multiplied by large factors at almost all collisions, we find a behavior again very similar to that of the Lorentz gas. In the other regime, where the effect of a single collision on average is very small, we found that the maximal Lyapunov exponent scales as the product of the tracer particle collision frequency and the two-third power of the mass ratio $m/(m+M)$, up to logarithmic corrections. These logarithmic corrections are special for the hard-ball potential and do not occur for more realistic interactions. Moreover, we have shown that the positive Lyapunov exponents determined by the tracer dynamics may dominate the Lyapunov spectrum of the fully interacting system under conditions approaching the Rayleigh-flight limit, provided the density of tracer particles, or alternatively the ratio between system size and tracer radius, remains finite. Again, a gap appears in the Lyapunov spectrum between the largest Lyapunov exponents associated with the tracer particle and the rest of the spectrum.

The different tracer-dominated regimes are depicted in Fig. 12 as a function of the mass ratio M/m and the radius ratio A/a for two different densities of a two-dimensional fluid. The diagrams are qualitatively similar for a three-dimensional fluid. Figure 12 shows that the system is in a fluid-dominated regime if the tracer is very massive. Nevertheless, we observe in Fig. 12b that the tracer-dominated regimes extend toward larger masses at lower densities.

A comment is here in order about Brownian motion. In typical Brownian motion conditions, the tracer particle is much more massive than the fluid particles and, moreover, the mean free path of the fluid particles among themselves is much shorter than the radius of the Brownian particle. Under such conditions the maximal Lyapunov exponent of the full system usually is essentially the same as the fluid Lyapunov exponent, as seen in Fig. 12. Then the Brownian particle does not contribute significantly to the dynamical instability of the system and is a probe for the dynamics of the surrounding fluid. This is the case in typical Brownian-motion experiments. In order to observe the new effect of dominance of the dynamical instability by the Brownian particle one has to use a sufficiently rarefied gas as surrounding fluid, in order to approach to the Rayleigh-flight limit, as seen in Fig. 12b.

ACKNOWLEDGMENTS

It is our great pleasure to dedicate this paper to our friend Bob Dorfman to whom we owe so much. We want to thank him for sharing with us his interests in the kinetic theory of Brownian motion, in the deep connections between chaos theory and statistical mechanics, in 17th century Dutch painting and in many other important areas of life. The authors thank Professor G. Nicolis for support and encouragement in this research. The authors are supported financially by the National Fund for Scientific Research (F. N. R. S. Belgium), by the Université Libre de Bruxelles, and by the Interuniversity Attraction Pole program of the Belgian Federal Office of Scientific, Technical and Cultural Affairs. H.v.B. also acknowledges support by the Mathematical physics program of FOM and NWO/GBE.

---

[1] J. R. Dorfman, *An Introduction to Chaos in Nonequilibrium Statistical Mechanics* (Cambridge University Press, Cambridge UK, 1999).

[2] Ch. Dellago, H. A. Posch, and W. G. Hoover, Phys. Rev. E **53**, 1485 (1996).

[3] H. van Beijeren and J. R. Dorfman, Phys. Rev. Lett. **74**, 4412 (1995); chao-dyn/9412012

[4] H. van Beijeren, J. R. Dorfman, H. A. Posch, and Ch. Dellago, Phys. Rev. E **56**, 5272 (1997); chao-dyn/9706019

[5] H. van Beijeren, A. Latz, and J. R. Dorfman, Phys. Rev. E **57**, 4077 (1998); chao-dyn/9711008
[6] R. van Zon, H. van Beijeren, and Ch. Dellago, Phys. Rev. Lett. **80**, 2035 (1998); chao-dyn/9710020
[7] R. van Zon, H. van Beijeren, J. R. Dorfman, Kinetic Theory Estimates for the Kolmogorov-Sinai Entropy and the Lyapunov Exponents for Dilute, Hard-Ball Gases and for Dilute, Random Lorentz Gases, in: *Hard Ball Systems and the Lorentz Gas*, D. Szasz Editor, Encyclopaedia of Mathematical Sciences (Springer, Berlin, 2000), pp. 233-278; chao-dyn/9909034
[8] R. van Zon, H. van Beijeren, J. R. Dorfman, Kinetic Theory of Dynamical Systems, in the Proceedings of the 1998 NATO-ASI *Dynamics: Models and Kinetic Methods for Non-equilibrium Many-Body Systems*, J. Karkheck Editor (Kluwer, Dordrecht, 2000) pp. 131-167; chao-dyn/9906040
[9] H. van Beijeren, A. Latz, and J. R. Dorfman, Phys. Rev. E **63**, 016312 (2001) *14 pages*; CD/0008027
[10] D. J. Evans, E. G. D. Cohen, and G. Morriss, Phys. Rev. A **42**, 5990 (1990).
[11] P. Gaspard and G. Nicolis, Phys. Rev. Lett. **65**, 1693 (1990).
[12] J. R. Dorfman and P. Gaspard, Phys. Rev. E **51**, 28 (1995).
[13] P. Gaspard, *Chaos, Scattering, and Statistical Mechanics* (Cambridge University Press, Cambridge UK, 1998).
[14] Matthieu Louis, *Chaos Microscopique dans un Modèle de Mouvement Brownien* (Mémoire de licence en sciences physiques, Université Libre de Bruxelles, 1999); P. Gaspard, Bull. Cl. Sci. Acad. Roy. Belg., series 6, tome **XI**, 9 (2000); P. Gaspard, Int. J. Mod. Phys. B **15**, 209 (2001).
[15] L. Nasser and J. R. Dorfman, unpublished.
[16] Ya. G. Sinai, Russian Math. Surveys **25**, 137 (1970).
[17] N. N. Krylov, Nature **153**, 709 (1944); N. N. Krylov, *Works on the Foundations of Statistical Mechanics* (Princeton University Press, 1979); Ya. G. Sinai, *ibid.* p. 239.
[18] J. J. Erpenbeck and W. W. Wood, in: B. J. Berne, Editor, *Statistical Mechanics, Part B: Time-Dependent Processes* (Plenum Press, New York, 1977) pp. 1-40.
[19] P. Gaspard and J. R. Dorfman, Phys. Rev. E **52**, 3525 (1995).
[20] H. A. Lorentz, Arch. Néerl. **10**, 336 (1905) [reprinted in Collected Papers vol. 3, p. 180].
[21] H. van Beijeren, Rev. Mod. Phys. **54**, 195 (1982).
[22] Lord Rayleigh (J. W. Strutt), Philos. Mag. 5, **32**, 424 (1891) [reprinted in Sci. Pap. **3**, 473 (Cambridge University Press, Cambridge UK)].
[23] H. Spohn, Rev. Mod. Phys. **52**, 569 (1980).
[24] R. van Zon, Phys. Rev. E **60**, 4158 (1999); cond-mat/9905027

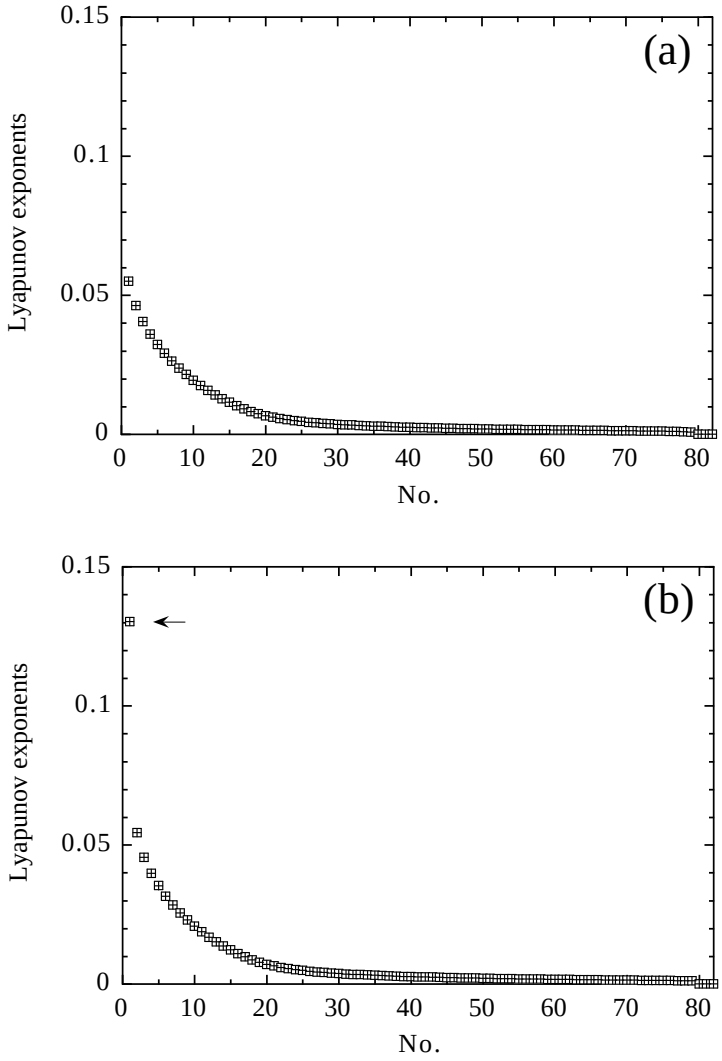

FIG. 1. Lyapunov spectra of a 2d fluid of density $n = 10^{-3}$ and temperature $T = 1$ composed of $N_{\rm f} = 40$ hard disks of radius $a = 1/2$ and mass $m = 1$ with $N_{\rm t} = 1$ hard disk of radius $A = 1/6$ and mass: (a) $M = 10$; (b) $M = 10^{-2}$. The squares depict the positive exponents and the crosses are minus the negative exponents.

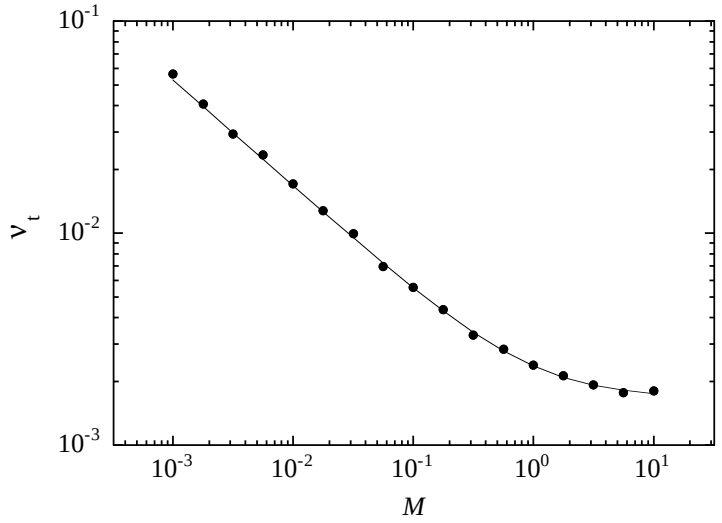

FIG. 2. Collision frequency $\nu_{\rm t}$ of the tracer particle in a 2d fluid of density $n = 10^{-3}$ and temperature $T = 1$ composed of $N_{\rm f} = 40$ hard disks of radius $a = 1/2$ and mass $m = 1$ with $N_{\rm t} = 1$ hard disk of radius $A = 1/6$ and varying mass M. The filled circles are the numerical data. The solid line is the prediction of Eq. (30) (see Table I).

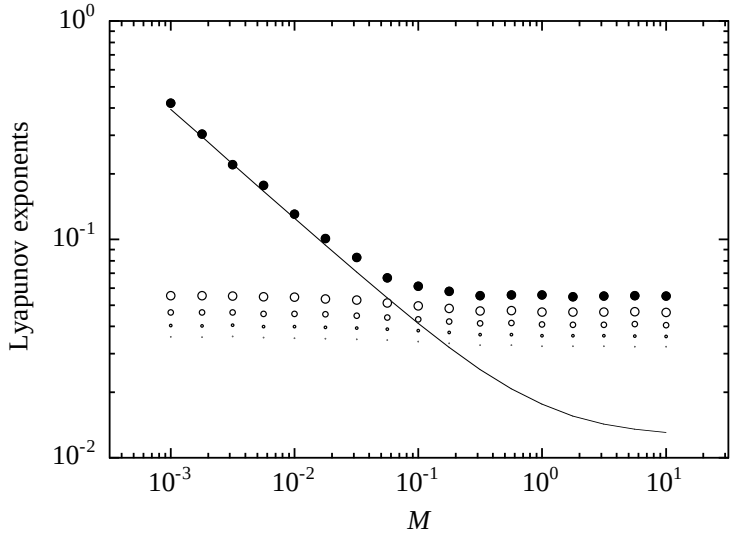

FIG. 3. The five largest Lyapunov exponents of a 2d fluid of density $n = 10^{-3}$ and temperature $T = 1$ composed of $N_{\rm f} = 40$ hard disks of radius $a = 1/2$ and mass $m = 1$ with $N_{\rm t} = 1$ hard disk of radius $A = 1/6$ and varying mass M. The filled circles depict the largest Lyapunov exponent and the open circles the four next ones. The solid line is the prediction of Eq. (46).

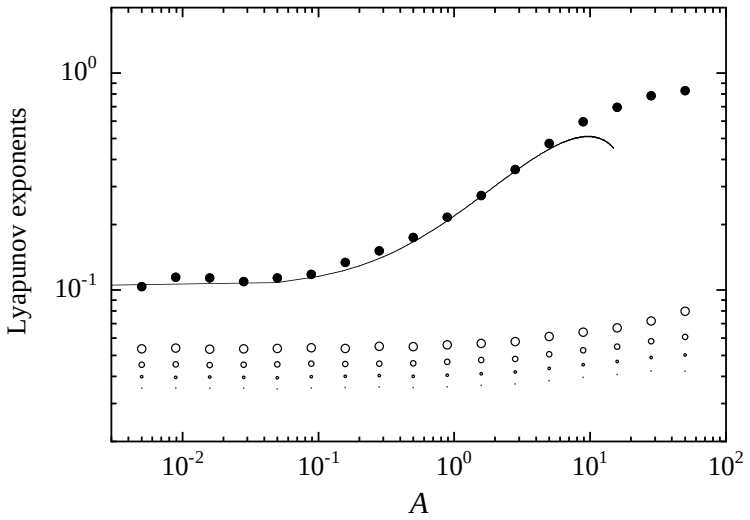

FIG. 4. The five largest Lyapunov exponents of a 2d fluid of density $n = 10^{-3}$ and temperature $T = 1$ composed of $N_{\rm f}$ hard disks of radius $a = 1/2$ and mass $m = 1$ with $N_{\rm t} = 1$ hard disk of varying radius A and mass $M = 10^{-2}$ ($N_{\rm f} = 40$ for $A < 10$, $N_{\rm f} = 39$, 37, and 31 for the last three values of $A > 10$). The filled circles depict the largest Lyapunov exponent and the open circles the four next ones. The solid line is the prediction of Eq. (46).

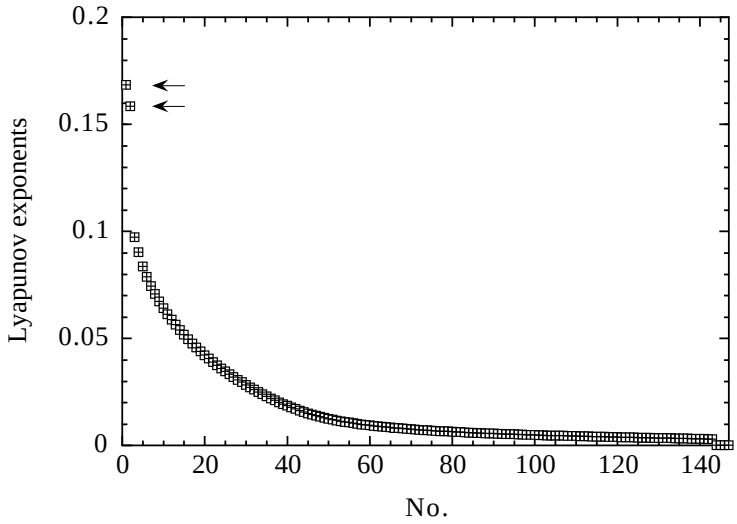

FIG. 5. Lyapunov spectrum of a 3d fluid of density $n = 10^{-3}$ and temperature $T = 1$ composed of $N_{\rm f} = 48$ hard spheres of radius $a = 1/2$ and mass $m = 1$ with $N_{\rm t} = 1$ hard sphere of radius $A = 1/6$ and mass $M = 10^{-2}$. The squares depict the positive exponents and the crosses are minus the negative exponents.

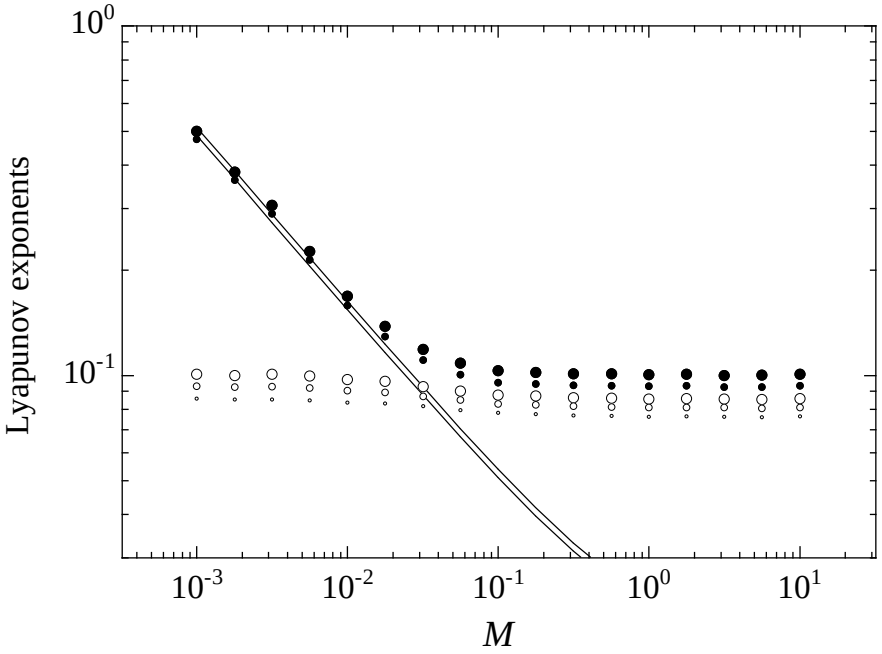

FIG. 6. The five largest Lyapunov exponents of a 3d fluid of density $n = 10^{-3}$ and temperature $T = 1$ composed of $N_{\rm f} = 48$ hard spheres of radius $a = 1/2$ and mass $m = 1$ with $N_{\rm t} = 1$ hard sphere of radius $A = 1/6$ and varying mass M. The filled circles depict the two largest Lyapunov exponents and the open circles the three next ones. The solid lines are the predictions of Eqs. (47) and (48).

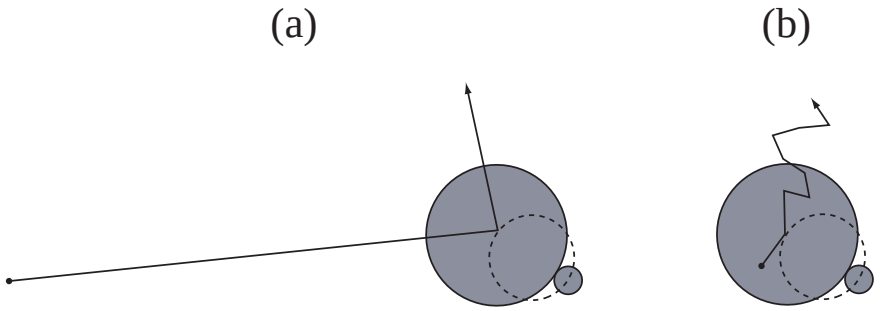

FIG. 7. Typical geometry of two successive collisions of the tracer particle when: (a) $\ell_{\rm t} \gg A + a$; (b) $\ell_{\rm t} \ll A + a$. The trajectories are depicted in the frame where the fluid particle is at rest.

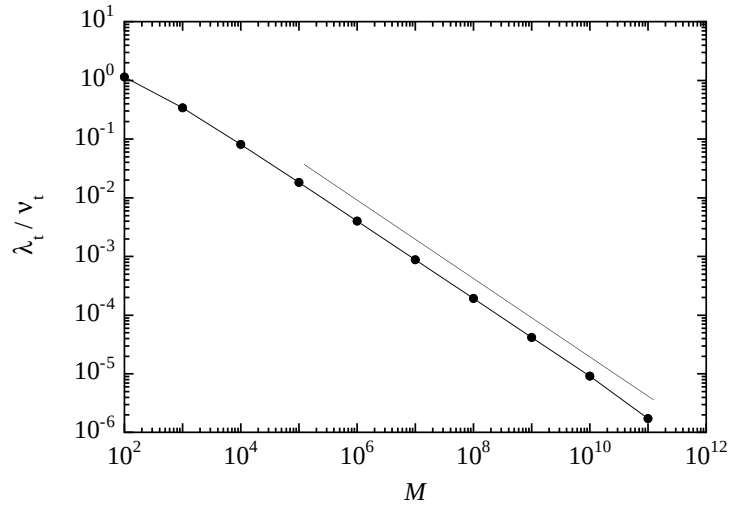

FIG. 8. Ratio of the maximal Lyapunov exponent λ_t to the collision frequency ν_t versus the mass M for a tracer disk of radius $A = 499.5$ in Rayleigh flight in the regime $\gamma \ll 1$. The Lyapunov exponent is calculated by Monte-Carlo simulation by assuming that the tracer particle undergoes independent successive random collisions from fluid disks of radius $a = 0.5$ and mass $m = 1$ at density $n = 10^{-8}$ and temperature $T = 1$. The straight line has the theoretically expected slope 2/3.

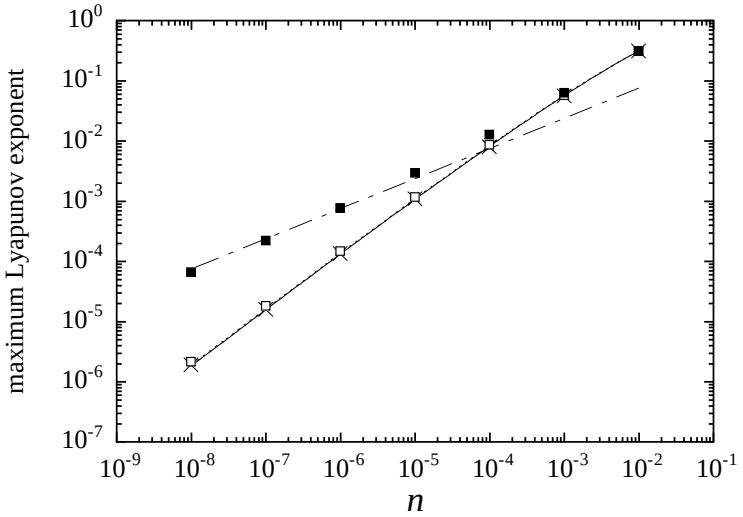

FIG. 9. maximal Lyapunov exponent of a 2d fluid of temperature $T = 1$ and varying density n containing $N_f \simeq 40$ hard disks of radius $a = 1/2$ and mass $m = 1$ with one tracer disk of radius A and mass M in the three cases (92). In the reference case $A = 1$ and $M = 1$, the maximal Lyapunov exponent λ_1 is depicted by the crosses and the fit by the solid line. In the case $A = 5$ and $M = 100$, λ_1 is depicted by the open squares and the fit by the dashed line. In the case $A = 1/(2\sqrt{n})$ and $M = 10$, λ_1 is depicted by the filled squares. The long-short dashed line is the fit $\lambda_1 = 0.75\sqrt{n}$.

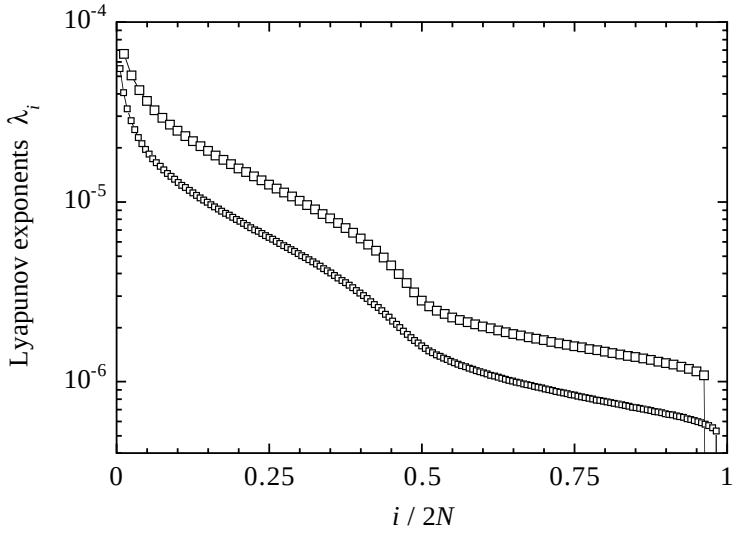

FIG. 10. Lyapunov spectra of a 2d fluid of temperature $T = 1$ and density $n = 10^{-8}$ containing respectively $N_{\rm f} = 39$ (large squares) and $N_{\rm f} = 83$ (small squares) hard disks of radius $a = 1/2$ and mass $m = 1$ with one tracer disk of radius $A = 5000$ and mass $M = 10$ as a function of the relative index $i/(2N)$ of the Lyapunov exponents λ_i.

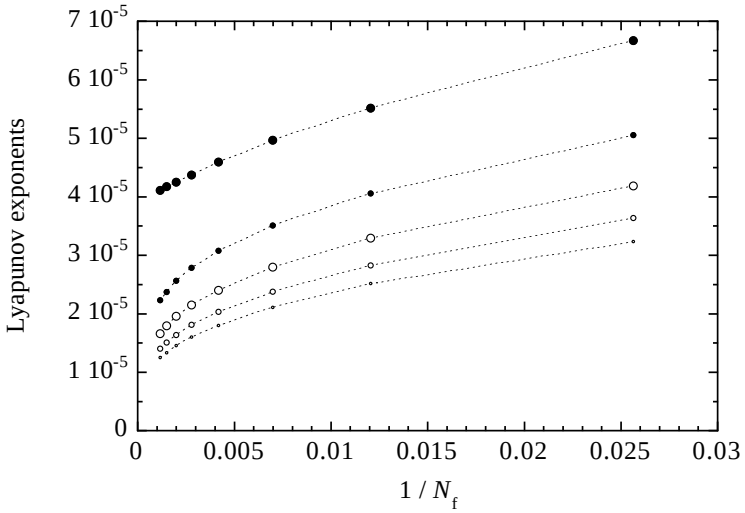

FIG. 11. The five largest Lyapunov exponents of a 2d fluid of temperature $T = 1$ and density $n = 10^{-8}$ containing a varying number $N_{\rm f} = 39, 83, 143, 239, 359, 503, 671, 863$ of hard disks of radius $a = 1/2$ and mass $m = 1$ with one tracer disk of radius $A = 5000$ and mass $M = 10$ versus $1/N_{\rm f}$. The Rayleigh-flight value of the maximal Lyapunov exponent is $\lambda_{\rm t} \simeq 3.3\ 10^{-5}$.

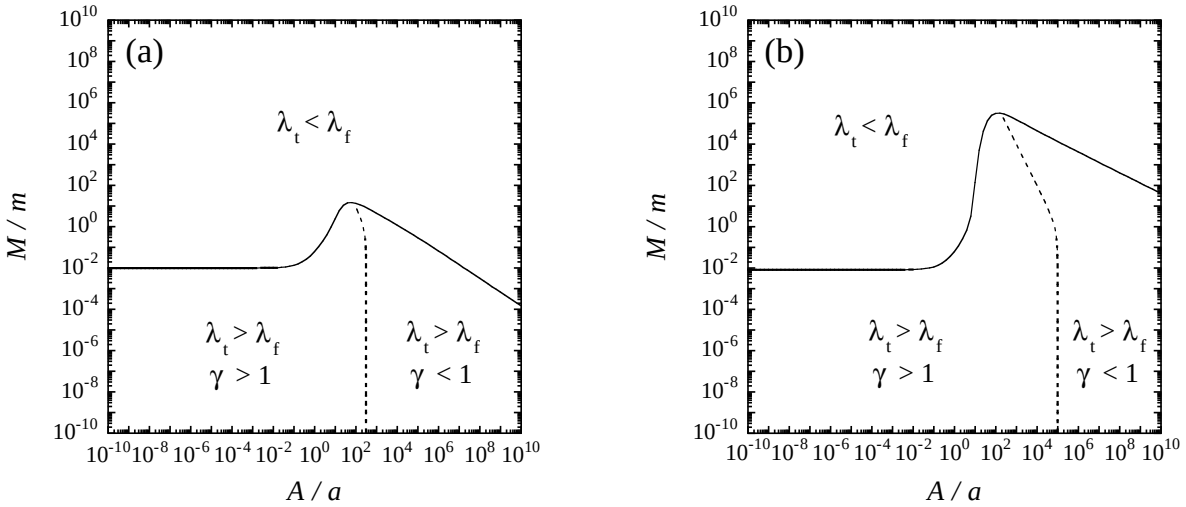

FIG. 12. Diagrams of the different regimes of the $d = 2$ systems composed of a tracer particle of radius A and mass M in a fluid of particles of radius a and mass m at density (a) $n = 10^{-5}$ and (b) $n = 10^{-10}$ and temperature $T = 1$. The area above the solid line shows the fluid-dominated regime with $\lambda_f > \lambda_t$. The areas below the solid line show the tracer-dominated regimes with $\lambda_t > \lambda_f$. The area on the lower left-hand side is the tracer-dominated regime with $\gamma > 1$, while the area on the lower right-hand side is the tracer-dominated regime with $\gamma < 1$. The Lorentz-gas limit is the part of the lower area where $M \ll m$.